Estimation of Soft Tissue Mechanical Parameters from Robotic Manipulation Data

Pasu Boonvisut, **Russell Jackson**, and **M. Cenk Çavuşoğlu**
Department of Electrical Engineering and Computer Science, Case Western Reserve University, Cleveland, OH 44106, USA

Pasu Boonvisut: bpasu@case.edu; Russell Jackson: rcj33@case.edu; M. Cenk Çavuşoğlu: cavusoglu@case.edu

Abstract

Robotic motion planning algorithms used for task automation in robotic surgical systems rely on availability of accurate models of target soft tissue's deformation. Relying on generic tissue parameters in constructing the tissue deformation models is problematic; because, biological tissues are known to have very large (inter- and intra-subject) variability. A priori mechanical characterization (e.g., uniaxial bench test) of the target tissues before a surgical procedure is also not usually practical. In this paper, a method for estimating mechanical parameters of soft tissue from sensory data collected during robotic surgical manipulation is presented. The method uses force data collected from a multiaxial force sensor mounted on the robotic manipulator, and tissue deformation data collected from a stereo camera system. The tissue parameters are then estimated using an inverse finite element method. The effects of measurement and modeling uncertainties on the proposed method are analyzed in simulation. The results of experimental evaluation of the method are also presented.

I. INTRODUCTION

Robotic motion planning algorithms being developed to enable robotic surgical assistants (RSAs) to perform certain surgical tasks autonomously while minimizing the damage to the tissue and errors in the operation rely on availability of accurate models of target tissues' deformation. As biological tissues are known to have very large inter- and intra-subject variability, construction of tissue deformation models using generic tissue parameters is not desirable. However, a priori mechanical characterization of the target tissues before a surgical procedure is also not practical. In this paper, a method for estimating the mechanical parameters of manipulated soft tissue from sensory data collected during robotic surgical manipulation is presented. The proposed method does not rely on specialized equipment, sensors, or characterization procedures. Instead, the method uses data collected during typical surgical manipulations, such as, grabbing and retracting the tissue, from a force sensor mounted on the robotic manipulator and a stereo camera system to estimate the tissue parameters. Specifically, the method uses an inverse finite element method to estimate the parameters of a nonlinear hyper-elastic material model so as to match the estimated tissue response to measured data (Sections III and IV). Several challenge scenarios were used to explore the sensitivity of the iterative inverse finite element scheme and the objective function based on uncertainties resulting from RSAs' sensing (Section V-A). Results from experimental evaluation and validation of the method are also presented (Section V-B).

II. BACKGROUND

Research on motion planning algorithms for robotic manipulators has traditionally concentrated on manipulation of rigid objects. However, recently, motion planning algorithms for manipulation of deformable objects have started to receive attention in the literature (e.g., [1–8]).

The robotic motion planning algorithms for manipulation of deformable objects use models of tissue deformation to estimate the behavior of the object under constraints resulting from the manipulation. Nonlinear finite element models based on continuum mechanics are widely used in many surgery simulations (e.g., [9–11]) to estimate large deformations accurately. In general, finite element methods give higher accuracy at the cost of increased computation. To avoid the computational costs of complex nonlinear finite element methods, Müller et al. [12] proposed a linear finite element method with co-rotational support to improve the simulation accuracy under large deformations. However, nonlinear finite element methods are preferred when the accuracy outcomes are needed to perform in surgical simulation [10, 11].

Different tissue models have been used to characterize the hyper-elastic deformable object behavior, such as St. Venant–Kirchhoff [13], Veronda–Westmann [10, 11, 14, 15], Arruda–Boyce [16], Neo–Hooke [10, 11], etc.

Traditionally, the parameter sets of different models are examined by performing uniaxial tests. Researchers find the set of parameters that match stress–strain relationship from experiments according to their strain energy model [14]. Recently, iterative parameters identifications using inverse finite element analysis have been proposed to determine the set of parameters. Mehrabian and Samani [15] estimated the set of parameters for tissue modeled using Veronda-Westmann model by performing uniaxial compression test on polyvinyl alcohol phantom. Sangpradit et al. [16] identified the parameters of Arruda-Boyce model by using wheeled probe indentation on a General Electric RTV6166 silicone phantom.

One of the differences between the present study and the earlier studies in the literature is that the parameter estimation scheme presented here does not require any specialized apparatus (such as those used by [17–19]), motions, or procedures (such as the performance of a uniaxial loading test [15]).

Most parameter estimation studies have been focused on simple motions such as indentations [16, 20–23] and geometrical tension, compression, and shear test [24, 25]. The published results for more complicated motions were lacking.

Instead, the proposed estimation scheme uses data collected during typical surgical manipulation motions of the manipulator (such as during retraction of the tissue by a gripper). Also, in the present study, the deformations of the object surface at multiple points were used in the estimation (similar to [24] which used movements of multiple points inside the tissue as observed through magnetic resonance imaging and which fitted non-linear material to measured force-displacement samples [21]), unlike earlier studies in the literature that rely on collocated force-displacement measurements (e.g., [16, 26]).

III. TISSUE MODELS

In this study, nonlinear finite element models were used to model the deformation of the soft tissues. Nonlinear finite element model stated here means the strain tensor as well as the stress–strain relationship are nonlinear (i.e., both geometric and material nonlinearities are

included). For simplification, the analyses were performed for the quasi-static case, neglecting the inertial and damping effects in the tissue dynamics. This is not a restrictive assumption, since manipulation velocities and bandwidths are small in typical surgical manipulations. The finite element simulations were performed using the `Salmon` finite element simulation package [11].

Strain energy density function (SEDF) *W* is a function that relates the Cauchy-Green deformation tensor *C* of the material to the to the strain energy density, and is used to characterize nonlinear stress-strain relationship of isotropic hyper-elastic materials. In this study, the Neo-Hookean nonlinear material model was used as the underlying material type. The Neo-Hookean model is a generalization of the St. Venant Kirchoff model [11] and does not have the element inversion problem [27].

The advantage of using Neo-hookean material is it captures the nonlinear nature of material while its parameters still have good physical interpretation. However, it is important to note that the use of the Neo-Hookean material type is not a requirement to the proposed parameter estimation scheme, which will be introduced in section IV-A. Different material type can be substituted without any major change to the method.

The SEDF and stress tensor of the Neo-Hookean material model are given by are given by

$$W = \frac{1}{2} \left(\mu(i_1 - 3) - \mu \log(i_3) + \lambda (\sqrt{i_3} - 1)^2) \right), \quad (1)$$

and

$$S = \mu I - \mu C^{-1} + \lambda (\sqrt{i_3} - 1) \sqrt{i_3} C^{-1}, \quad (2)$$

respectively [10, 11].

In here, λ and μ, are the Lamé's first and second parameters respectively, which can be calculated from Young's modulus *E* and Poisson's ratio *v* of the material by using the relationship

$$\lambda = \frac{E\nu}{(1+\nu)(1 - 2\nu)}, \quad (3)$$

$$\mu = \frac{E}{2(1+\nu)}. \quad (4)$$

i_1, i_2 and i_3 are the invariants of the Cauchy-Green deformation tensor *C* which are defined by

$$i_1 = \text{trace}(C), \quad (5)$$

$$i_2 = \frac{1}{2} \left(\text{trace}(C)^2 - \text{trace}(C^2) \right), \quad (6)$$

$$i_3 = \det(C). \quad (7)$$

IV. PARAMETER ESTIMATION SCHEME

The inputs to the parameter estimation algorithm are the initial geometry of the deformable object (obtained from preoperative medical imaging), the motion of the robotic end-effector grabbing the tissue (given by the joint sensors and kinematics of the robotic manipulator), the tissue interaction forces measured at the robotic end-effector (measured by a 6 axis force/torque sensor mounted on the manipulator), and the motions of a set of fiducials on the surface of the deformable object (measured by a stereo camera system). The robotic end-effector motions, tissue interaction forces, and the motion of the fiducials are assumed to be synchronously recorded trajectories.

The operation of the parameter estimation algorithm is summarized in Fig. 1 and Fig. 2. The algorithm starts by an initial estimate of the mechanical parameters of the target tissue being manipulated (Fig. 1). Using the estimated mechanical parameters, the simulation loop calculates the deformations of the tissue using a finite element model of the tissue subject to the boundary conditions resulting from specified motion of the robotic end-effector grabbing the tissue. The simulation loop then returns the estimates of the interaction forces and the motions of the fiducials during the manipulation. These estimated interaction force and fiducial motion trajectories are then compared with the actual trajectories observed by the sensors by using an objective function (described in section IV-A), and checked for convergence. If the objective function has not converged, the estimates of the parameters are updated, and the new parameters are fed back into the simulation loop.

The nonlinear finite element is employed in the simulation loop. The manipulator's initial configuration, the initial tissue geometry and the estimated tissue parameters are used by the nonlinear finite element simulator to solve for the deformation of the tissue in quasi-static state. Deformation of the tissue in subsequent time steps is then iteratively calculated by using the nonlinear finite element model. At each time step, the configuration of the tissue at the end of the last time step is used as the initial tissue configuration, and the boundary conditions are updated based on the corresponding configuration of the end-effector. The trajectories of the interaction forces and the locations of the fiducials on the tissue surface are calculated from the simulation results and are used to evaluate the objective function.

A. The Objective Function

The inverse finite element analysis is used to find the set of tissue's parameters that fits the observations. Two different sets of observations are collected from the sensory system. The first set of observations is the interaction forces between the end-effector and tissue during the surgical manipulation. The second set of observations is the trajectories of the points of interest fiducials identified on the surface of the tissue. Young's modulus and Poisson's ratio are the set of parameters that specify the tissue's mechanical properties, for the material type used in this study (see section III). The objective function then has two terms. The first term is a position sensitive term (similar to [21]) and the second term is a force sensitive term. The objective function is then defined as

$$\underset{E,\nu}{\operatorname{argmin}} \|\boldsymbol{x}_{\mathrm{s}}(E,\nu) - \boldsymbol{x}_{\mathrm{o}}\|^2 + \mathscr{C}\|\boldsymbol{f}_{\mathrm{s}}(E,\nu) - \boldsymbol{f}_{\mathrm{o}}\|^2, \quad (8)$$

where the subscripts s and o denote, respectively, the simulation and observed outputs, $\boldsymbol{f}$ is the vector representing the forces exerted on the RSA's gripper, and $\boldsymbol{x}$ is the vector representing the trajectories of the points of interest's positions, and $\mathscr{C}$ is the scaling factor used to match the scales of the force and position variables.

If desired, the scaling factor can be biased to favor one of the two terms. However, in this study, instead of using a prescribed set value, the scaling factor is automatically determined for each estimate problem as

$$\mathscr{C}_e = \frac{\max\limits_{E,\nu}\|\boldsymbol{x}_s - \boldsymbol{x}_o\|^2 - \min\limits_{E,\nu}\|\boldsymbol{x}_s - \boldsymbol{x}_o\|^2}{\max\limits_{E,\nu}\|\boldsymbol{f}_s - \boldsymbol{f}_o\|^2 - \min\limits_{E,\nu}\|\boldsymbol{f}_s - \boldsymbol{f}_o\|^2}. \quad (9)$$

This $\mathscr{C}e$ scales both terms equally in the parameter region of interest. Assuming that the tissue simulations always have errors in the force term, the scaling factor will be always well-defined. In (9) both of the max terms are estimated by sampling the region of interest of the parameters while the min terms are determined by performing numerical minimizations.

V. METHODS

A. Simulation Methods

In this section, results of the simulation studies of the proposed method are presented. Several different simulation scenarios were used to validate the proposed scheme, and explore its performance under various types of uncertainties.

A limitation of in vivo tissue manipulation is that it is difficult to acquire the true state of the tissue to initialize computations and it has greater uncertainties compared to ex vivo tests.

The first simulation scenario assumed that the tissue and manipulation geometries were acquired accurately. The second scenario considered the case when the tissue geometry was not perfectly modeled. The third scenario considered the case when there were uncertainties in positioning of the end-effector on the target tissue. And finally, the fourth scenario considered uncertainties in robots motion.

In the simulations a tissue model in the shape of a square patch, shown in Fig. 3, with dimensions $10 \times 10 \times 1$ cm was used. The center of the tissue was (0.0,0.0,0.0) in x-y-z coordinate. The end-effector gripper was assumed to grasp a 2×2 cm area on the tissue without any slip. This was modeled by anchoring the grabbed part of the tissue rigidly to the gripper by position boundary conditions. The size of the gripper was 2 cm in width and initially at (0.04,0.0,0.0) m. The tissue was assumed to be anchored on the left sides; and, the gripper retracted the tissue by pulling in the direction of the arrow shown in Fig. 3. The stress and strain of the tissue are assumed to be in zero state at the beginning of the experiment including the effect of gravity.

The `Salmon` [11] open source finite element modeling and simulation package was used as the underlying FEM simulation engine, after custom modifications. The `Salmon` package offers FEM simulation with geometric and material nonlinearities. The meshing of the geometric models to use in the FEM simulations was done by TetGen [28].

The SQP algorithm using Quasi-Newton line search, as provided by the MATLAB's fmincon function, was used to find minimum of the objective function.

All experiments were conducted on a 2.93 GHz Intel® Core™ i7 CPU, and 12 GB of RAM. `Salmon` was implemented in the C++ language and MATLAB® was used to implement the optimization scheme.

In the simulation scenarios, all vision and force sensing i.e., the trajectories of the fiducials and the interaction forces, were assumed to be perfectly measured. The reference values of

the sensing data were computed from simulations of a finite element model with a higher density mesh, while the estimation of the set of parameters were be performed using a finite element model with a lower density mesh. Specifically, a mesh with 3122 nodes and 13473 elements was used to generate the sensing data, while a mesh with 991 nodes and 3595 elements was used in the estimation process, unless otherwise noted. The reference parameters were 15 kPa and 0.49 for Young's modulus and Poisson's ratio, respectively.

B. Experimental Methods

In the experiments, we used soft tissue phantom created using Ecoflex® 0030, a two–part silicone rubber with Silicone Thinner® (non-reactive silicone fluid), from Smooth-On Inc. which was used in [29]. The silicone phantoms with two different consistencies of Silicone Thinner (see table VI) were used in order to cover a wide range of parameter values.

The experimental setup is shown in Fig. 4. The tissue phantoms used in the experiments were similar in shape and size to the models used in the simulation studies described in section V-A. Specifically, the tissue phantoms were square in shape, with dimensions, $10 \times 10 \times 1$ cm. The tissue phantoms were placed horizontally on a flat lubricated surface anchored to a wall on their left side, while being grabbed and retracted by a gripper towards right. The retraction action was achieved by moving the gripper 10 steps, in 2 mm steps, towards right, producing a 10% elongation of the tissue phantom. 16 artificial fiducials were marked on the top surface of the tissue and were tracked by a calibrated stereo camera pair to measure their deformations during retraction. A Nano17 6 axis force/torque sensor (by ATI Industrial Automation, Apex, NC) was mounted between the gripper and the actuator to measure the manipulation forces. The force sensor outputs were recorded via a NI PCI–6023E multifunction data acquisition system.

The silicone surface was labeled with colored glass beads 2 mm in diameter which were used as the fiducials. The stereo camera pair was two of Point Gray Research (PGR) Flea 2 cameras which captured images at 640×480 pixels. The camera lenses focal length were 4.5 mm. The stereo camera pair had a inter-camera distance of 35.89 mm. The cameras were placed at distance of 20 cm to the tissue sample. The cameras were programmed using the (PGR) Flycapture library and OpenCV. The camera images were calibrated and rectified using stereo calibrate routines native to OpenCV [30]. The image is analyzed in HSV color space. The fiducial beads were detected using their color. Once the fiducials were detected, each individual fiducial location was calculated by distinguishing each fiducial in the image. After the fiducials were detected in the stereo image pair, the actual location of the fiducials was triangulated using the camera calibration information.

VI. RESULTS

A. Simulation Results

1) Accurate Tissue and Manipulation Geometry Acquisitions—The first set of simulation studies were conducted to validate if the proposed algorithm could accurately identify the tissue parameters under ideal conditions, specifically, when perfect information about the geometry of the specimen and the geometry of manipulation (i.e., motion of the end-effector relative to the target tissue) was available. The effect of the density of the finite element model mesh used in the estimation algorithm on the accuracy of the parameter estimation was also evaluated.

In case 1, the tissue model in the estimator was discretized into a higher density mesh. In case 2, the tissue model in the estimator was discretized into a lower density mesh.

The results in Table I show that the proposed method can accurately estimate the tissue parameters under low uncertainty conditions, and the accuracy of the method does not depend heavily on the mesh density (at least, at the range considered here). The parameters estimated in case 2 were reasonably close to the actual values while the complexity is tremendously lower. Therefore, in the subsequent studies (sections VI-A.2–VI-A.5), the low density mesh was used in estimation while the high density mesh was used to generate the simulated measurement data.

2) Uncertainties in Tissue Geometry—The second set of simulations was conducted to evaluate the effectiveness of the method when the tissue geometry was not perfectly modeled. This was evaluated by using reference meshes which were perturbed from the original shape, while using the original mesh with the smooth surface in the estimation algorithm. The high density mesh was used to generate the test data while the low density mesh (described above) was used in parameter estimation.

The rough surfaces in this work were generated using the ridged multifractal terrain algorithm [31] in MeshLab [32] to represent uncertainties in tissue geometry. The results reported in Table II shows the sensitivity of the scheme to the size of the perturbations, at varying 2%, 4% and 8% of the tissue's original thickness, as can be seen in Fig. 5.

The results demonstrated that the proposed algorithm still handled the problem quite well. Only the Young's modulus was estimated by the method was slightly off when the fractal was higher.

The algorithm that was used to generate fractal in the experiment also grew the tissue. That is the reason why Young's modulus estimated from the scheme increased as the perturbation level increased. It is difficult to model the tissue geometry perfectly in simulation; however, from the experiments, the model should be accurately modeled at around 5% of the tissue's original thickness.

3) Uncertainties in the Position of the Robot's Target—The third set of simulations was conducted to evaluate the effectiveness of the method when there were uncertainties in the positioning of the end-effector on the target tissue.

The simulations were done by randomly changing the center of the robot's target (the grasping point) with standard deviation of 5 mm, 10 mm and 20 mm (see Table III).

The algorithm results are acceptable when the grasping point is mislocated up to 10mm. For 20mm mislocation, the parameter reconstructed from the scheme had unacceptably large variation and especially Poisson's ratio had an unacceptably large error due to the wrong assumption of grasping location further to the anchor points.

4) Uncertainties from the Robot's Motion—This set of simulations was conducted to evaluate the effectiveness of the method when there were uncertainties in robot motions. The additive Gaussian noise was generated to study the effect of uncertainties at 10%, 20% and 50% noise levels (standard deviation of the Gaussian noise as a percent of the magnitude of the position control signal.) The results are shown in Table IV.

Noise from the control signal appears not to cause a significant effect on the parameter estimation if the noise level is not extremely high.

5) Parameter Estimation under Complex Motions—The merit of this multiaxial estimation framework over uniaxial estimation is the ability to estimate the tissue parameters

under complex surgical manipulations. This set of simulations was conducted to evaluate the effectiveness of the method when the robot had non-trivial motions during a surgical manipulation. Fig. 6 shows the five different motions used in the simulations. In the first test motion, the gripper diagonally pulled the tissue on the orthogonal plane in the horizontal and up direction. In the second case, the gripper diagonally pulled the tissue in the tissue plane. In the third case, the gripper horizontally pulled the tissue by simultaneously rotating the gripper. In the fourth case, the gripper pulled the tissue sideways in the tissue plane. And in the fifth and final case, the gripper pulled the tissue horizontally in the tissue plane while rotating the tissue to twist it.

The results in Table VI show that the method can still estimate the parameters with good accuracy under such complex motions.

B. Experimental Results

Different tissue consistencies were obtained by using different silicone rubber and silicone thinner proportions during the preparation of the phantoms. The parameter estimates for the two different tissue phantoms are reported in Table VI. For baseline comparison, the material parameters (Young's modulus and Poisson's ratio) reported in the literature for the Ecoflex 0030 for the 1:1:0 mixture proportions in [29] are 29.5 kPa and 0.5, respectively. (Actually, in [29] Poisson's ratio of 0.5 was assumed, not directly estimated). [1] These reported parameter values are very close to the values 27.24 kPa and 0.43 estimated here using the proposed method.

Fig. 7 and Fig. 8 show that the trajectories of fiducial positions and force profile start to deviate from the actual trajectories for large deformations, even though there is a good agreement between the estimated and actual trajectories for relatively smaller deformations. Neo-Hookean might not be the best choice for highly nonlinear materials in some cases.

VII. DISCUSSION AND CONCLUSIONS

This paper presented a new inverse nonlinear finite element based scheme to estimate the mechanical parameters of soft tissues using data collected during regular manipulation of the tissue in robotic surgery. The method uses a hyper-elastic material model for the tissue. Several challenge scenarios and different types of complex motions were considered to test the sensitivity of the proposed multiaxial framework scheme. Results of the method are evaluated and validated experimentally as well. The simulation and experimental results indicated that the proposed scheme is effective in estimating the parameters in general.

Typical surgical manipulation motions are relatively slow. Therefore, the tissue deformations and interactions forces can be approximated as quasi-static, ignoring the viscous and inertial effects.

It is also important to note that, the choice of the Neo-Hookean material type is not fundamental to the proposed method. The same overall tissue parameter estimation method can also be applied by using different underlying material types.

Acknowledgments

---

[1]To the best of our efforts, these were the only parameter values that we were able to find in the literature for the Ecoflex silicone.

References

1. Hirai S, Tsuboi T, Wada T. "Robust grasping manipulation of deformable objects". Lecture Notes in Computer Science. 2201:411–416.

2. Gopalakrishnan K, Goldberg K. "D-Space and deform closure grasps of deformable parts". The International Journal of Robotics Research. 2005; vol. 24(no. 11):899–910.

3. Moll M, Kavraki LE. "Path planning for deformable linear objects". IEEE Transactions on Robotics. Aug; 2006 vol. 22(no. 4):625–636.

4. Saha, M.; Isto, P. Proceedings 2006 IEEE International Conference on Robotics and Automation, 2006. ICRA 2006. IEEE; 2006. "Motion planning for robotic manipulation of deformable linear objects"; p. 2478-2484.

5. Saha M, Isto P. "Manipulation planning for deformable linear objects". IEEE Transactions on Robotics. Dec; 2007 vol. 23(no. 6):1141–1150.

6. Alterovitz R, Branicky M, Goldberg K. "Motion planning under uncertainty for image-guided medical needle steering". The International Journal of Robotics Research. Nov; 2008 vol. 27(no. 11–12):1361–1374. [PubMed: 19890445]

7. Alterovitz R, Goldberg KY, Pouliot J, Hsu IC. "Sensorless motion planning for medical needle insertion in deformable tissues". IEEE Transactions on Information Technology in Biomedicine. Mar; 2009 vol. 13(no. 2):217–225. [PubMed: 19126473]

8. Jansen, R.; Hauser, K.; Chentanez, N.; van der Stappen, F.; Goldberg, K. IEEE International Conference on Intelligent Robots and Systems (IROS). St Louis; Oct. 2009 "Surgical retraction of non-uniform deformable layers of tissue: 2D robot grasping and path planning".

9. Bro-nielsen M. "Finite element modeling in surgery simulation". Proceedings of the IEEE. 1998; vol. 86:490–503.

10. Wu, X. "Design of an interactive nonlinear finite element based deformable object simulator". 2002. Ph.D. dissertation, University of California at Berkeley

11. Nienhuys, H-W. "Cutting in deformable objects". 2003. Ph.D. dissertation, Utrecht University

12. Müller M, Dorsey J, McMillan L, Jagnow R, Cutler B. "Stable Real-Time deformations". ACM Press. 2002:49–54.

13. Barbi J, James DL. "Real-time subspace integration for St. Venant-Kirchhoff deformable models". ACM Transactions on Graphics (SIGGRAPH 2005). Aug; 2005 vol. 24(no. 3):982–990.

14. Veronda DR, Westmann RA. "Mechanical characterization of skin –finite deformations". Journal of Biomechanics. Jan; 1970 vol. 3(no. 1):111–124. [PubMed: 5521524]

15. Mehrabian, H.; Samani, A. "Constrained hyper-elastic parameters reconstruction of PVA (Polyvinyl Alcohol) phantom undergoing large deformation". In: Miga, MI.; Wong, KH., editors. Medical Imaging 2009: Visualization, Image-Guided Procedures, and Modeling. Vol. vol. 7261. Spie. 2009

16. Sangpradit, K.; Liu, H.; Seneviratne, LD.; Althoefer, K. 2009 IEEE International Conference on Robotics and Automation. IEEE; May. 2009 "Tissue identification using inverse finite element analysis of rolling indentation"; p. 1250-1255.

17. Ottensmeyer, MP. 2001. "Minimally invasive instrument for in vivo measurement of solid organ mechanical impedance". Ph.D. dissertation, Massachusetts Institute of Technology. Dept. of Mechanical Engineering

18. Kauer M, Vuskovic V, Dual J, Szekely G, Bajka M. "Inverse finite element characterization of soft tissues". Medical Image Analysis. 2002; vol. 6(no. 3)

19. Brouwer I, Ustin J, Bentley L, Sherman A, Dhruv N, Tendick F. "Measuring in vivo animal soft tissue properties for haptic modeling in surgical simulation". Stud Health Technol Inform. 2001; vol. 81:69–74. [PubMed: 11317820]

20. Lang J, Pai DK, Woodham RJ. "Acquisition of elastic models for interactive simulation". The International Journal of Robotics Research. Aug; 2002 vol. 21(no. 8):713–733.

21. Bickel, B.; Bächer, M.; Otaduy, MA.; Matusik, W.; Pfister, H.; Gross, M. ACM SIGGRAPH 2009 papers. New York, NY, USA: ACM; 2009. "Capture and modeling of non-linear heterogeneous soft tissue"; p. 1-9.ser. SIGGRAPH '09

22. Fong P. "Sensing, acquisition, and interactive playback of data-based models for elastic deformable objects". The International Journal of Robotics Research. May; 2009 vol. 28(no. 5): 630–655.

23. Frank B, Schmedding R, Stachniss C, Teschner M, Burgard W. "Learning the elasticity parameters of deformable objects with a manipulation robot". Oct.2010 :1877–1883.

24. Kerdok AE, Cotin SM, Ottensmeyer MP, Galea AM, Howe RD, Dawson SL. "Truth cube: Establishing physical standards for soft tissue simulation". Medical Image Analysis. Sep; 2003 vol. 7(no. 3):283–291. [PubMed: 12946469]

25. Gao Z, Lister K, Desai J. "Constitutive modeling of liver tissue: Experiment and theory". Annals of Biomedical Engineering. Feb; 2010 vol. 38(no. 2):505–516. [PubMed: 19806457]

26. d'Aulignac, D.; Çavu o lu, MC.; Laugier, C. MICCAI '99: Proceedings of the Second International Conference on Medical Image Computing and Computer-Assisted Intervention. London, UK: Springer-Verlag; 1999. "Modeling the dynamics of the human thigh for a realistic echographic simulator with force feedback"; p. 1191-1198.

27. Irving, G.; Teran, J.; Fedkiw, R. SCA '04: Proceedings of the 2004 ACM SIGGRAPH/ Eurographics symposium on Computer animation. Aire-la-Ville, Switzerland, Switzerland: Eurographics Association; 2004. "Invertible finite elements for robust simulation of large deformation"; p. 131-140.

28. Si H. Tetgen: A quality tetrahedral mesh generator and a 3D delaunay triangulator.

29. Hollenstein M. "Mechanical characterization of soft materials: Comparison between different experiments on synthetic specimens". Master's thesis, Institute of Mechanical Systems Department of Mechanical and Process Engineering, ETH Zurich. 2008

30. Bradski, G.; Kaehler, A. Learning OpenCV: Computer Vision with the OpenCV Library. 1st ed.. O'Reilly Media; Sep. 2008

31. Ebert, DS.; Musgrave, FK.; Peachey, D.; Perlin, K.; Worley, S. Texturing and Modeling, Third Edition: A Procedural Approach (The Morgan Kaufmann Series in Computer Graphics). 3rd ed.. Morgan Kaufmann; Dec. 2002
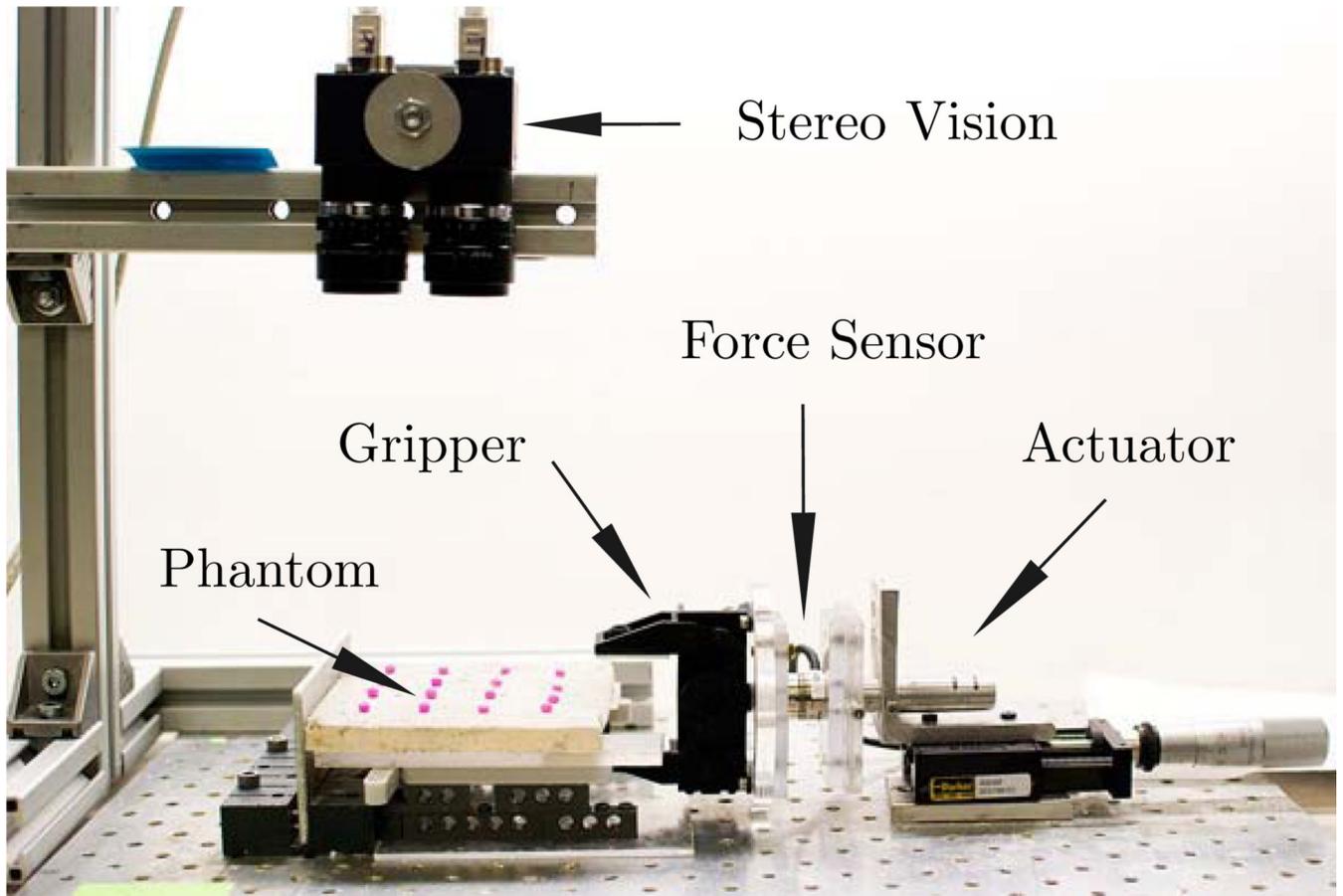
32. Cignoni P. MeshLab.
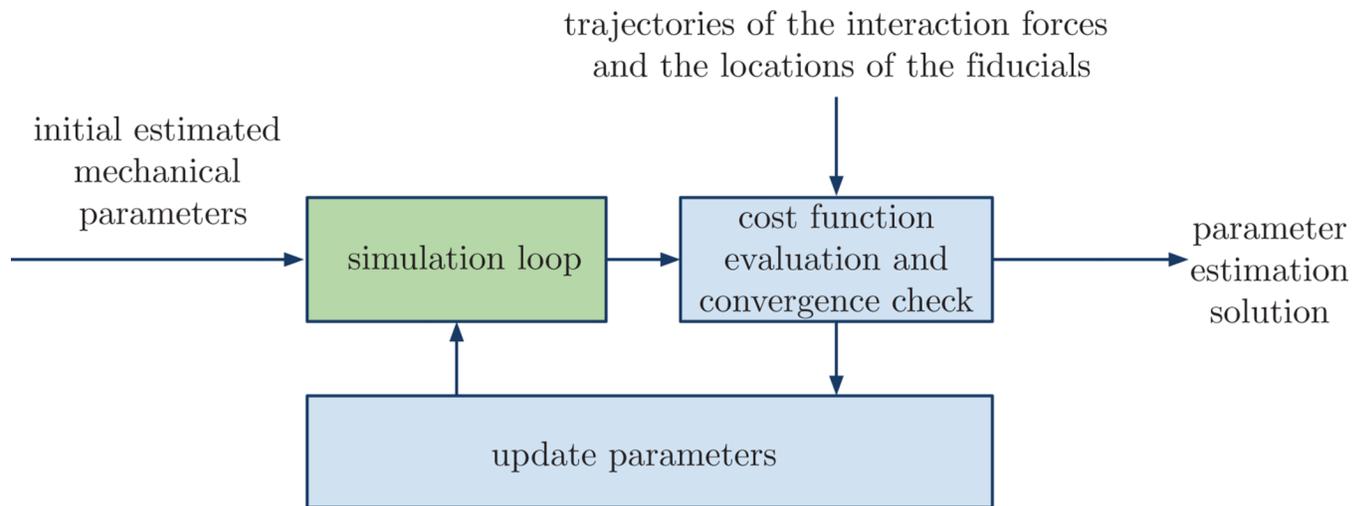
Fig. 1.
Flow chart describes the proposed iterative parameter determination scheme.
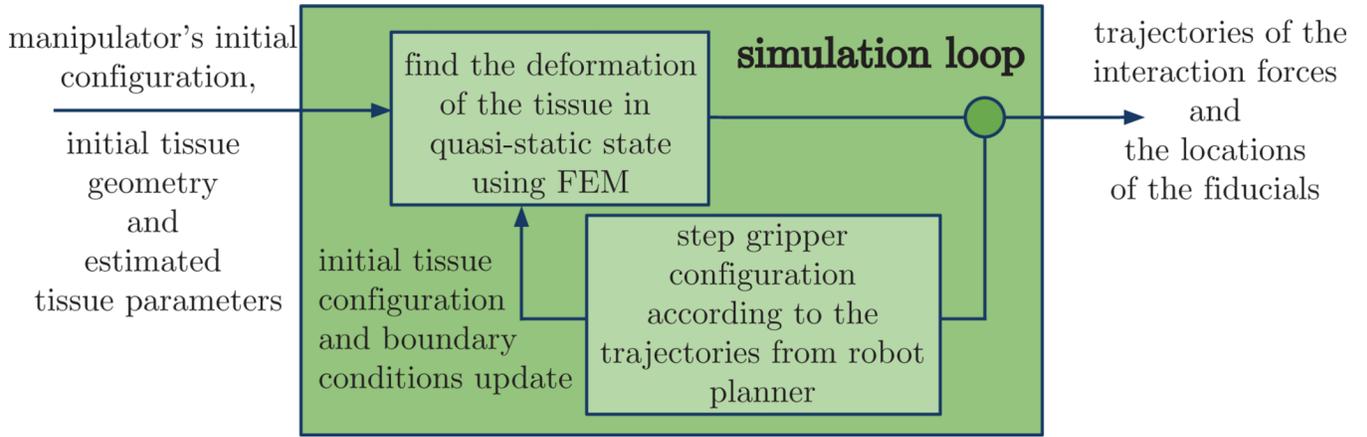
Fig. 2.
The diagram illustrates the simulation loop in Fig. 1
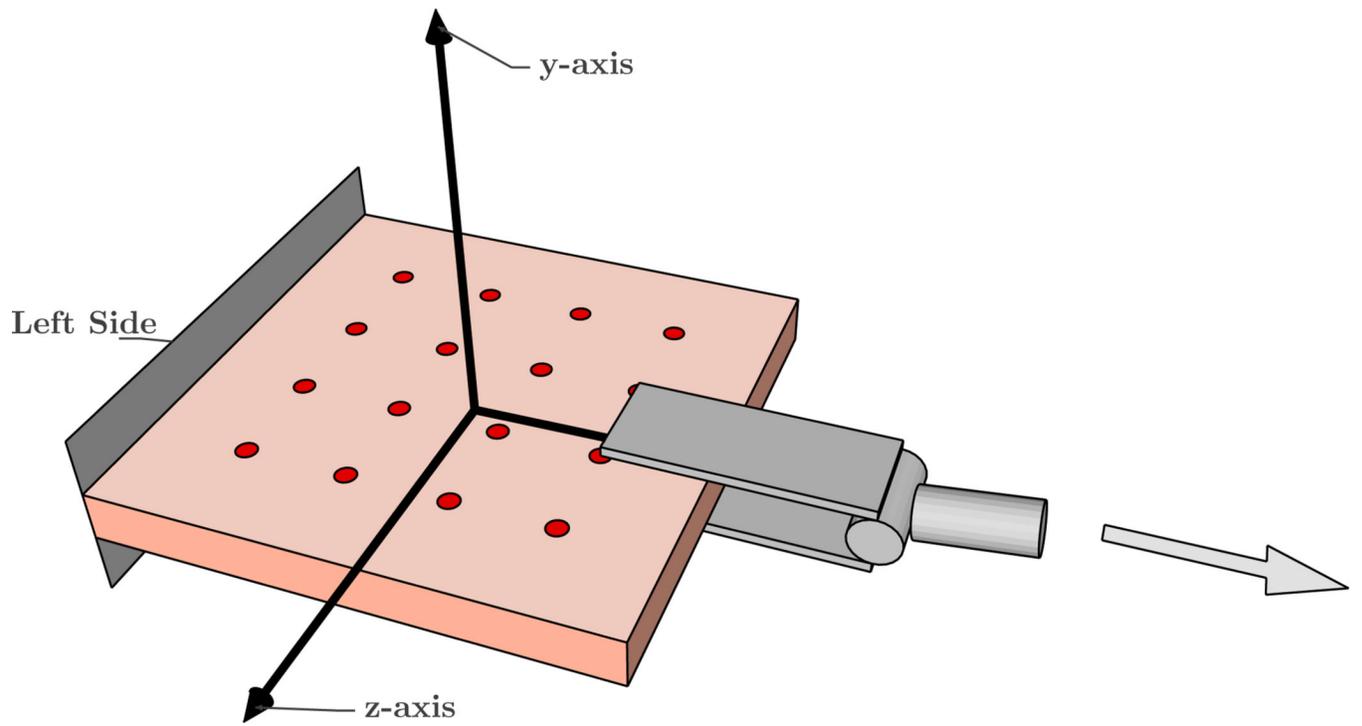
Fig. 3.
The setup of the experiment shows the gripper grasping on the right side of tissue and pulling in the direction of the arrow.

Fig. 4.
The physical experiment setup.

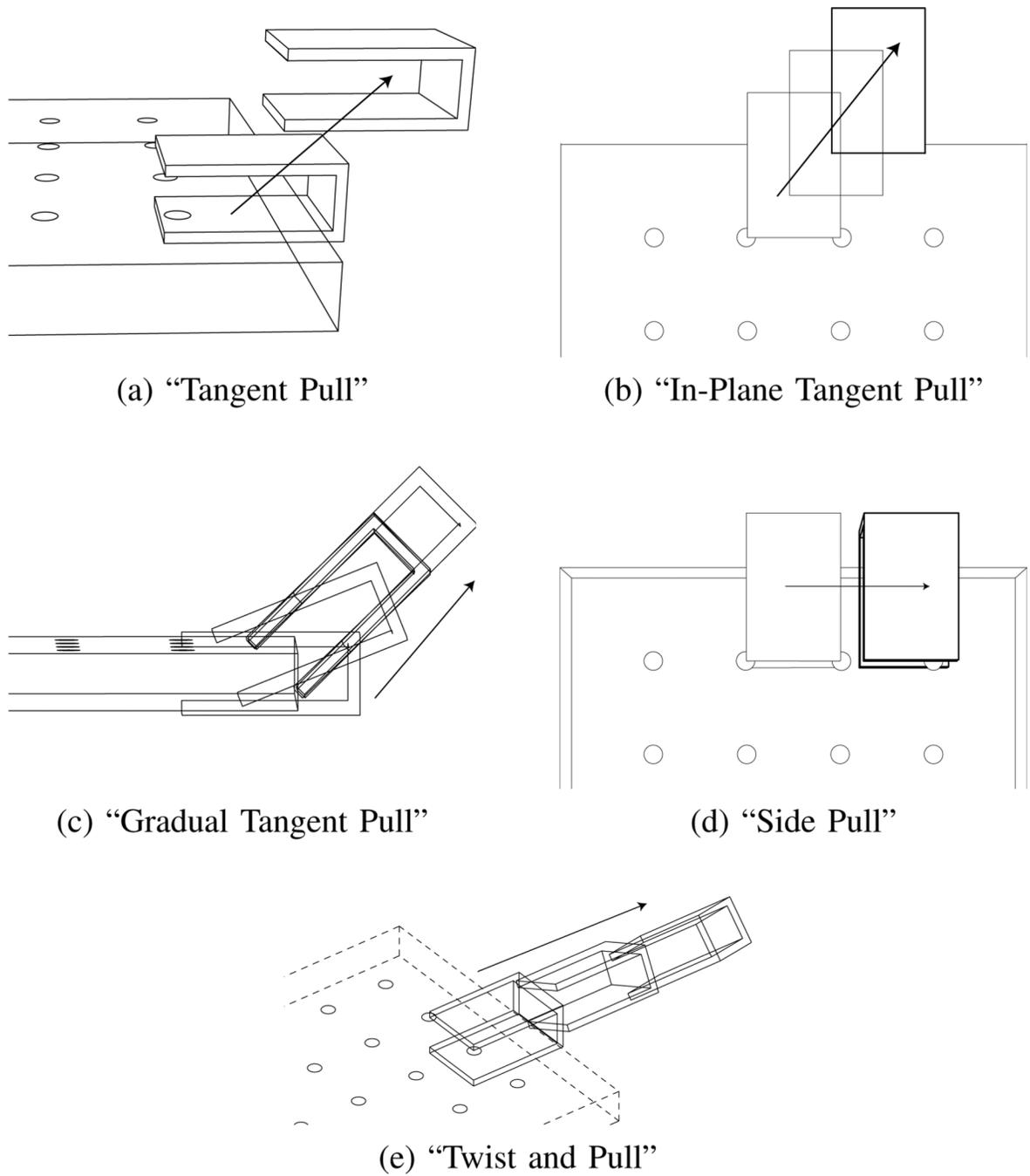(a) fractal maximum height scale of 2% of the tissue's original thickness

(b) fractal maximum height scale of 4% of the tissue's original thickness

(c) fractal maximum height scale of 8% of the tissue's original thickness

Fig. 5.
Unknown parameter tissue with rough surface generated using the ridged multifractal terrain algorithm [31].

(a) "Tangent Pull"

(b) "In-Plane Tangent Pull"

(c) "Gradual Tangent Pull"

(d) "Side Pull"

(e) "Twist and Pull"

Fig. 6.
Figures show the different types of complex end-effector motion used to evaluate the parameter estimation in section VI-A.5.
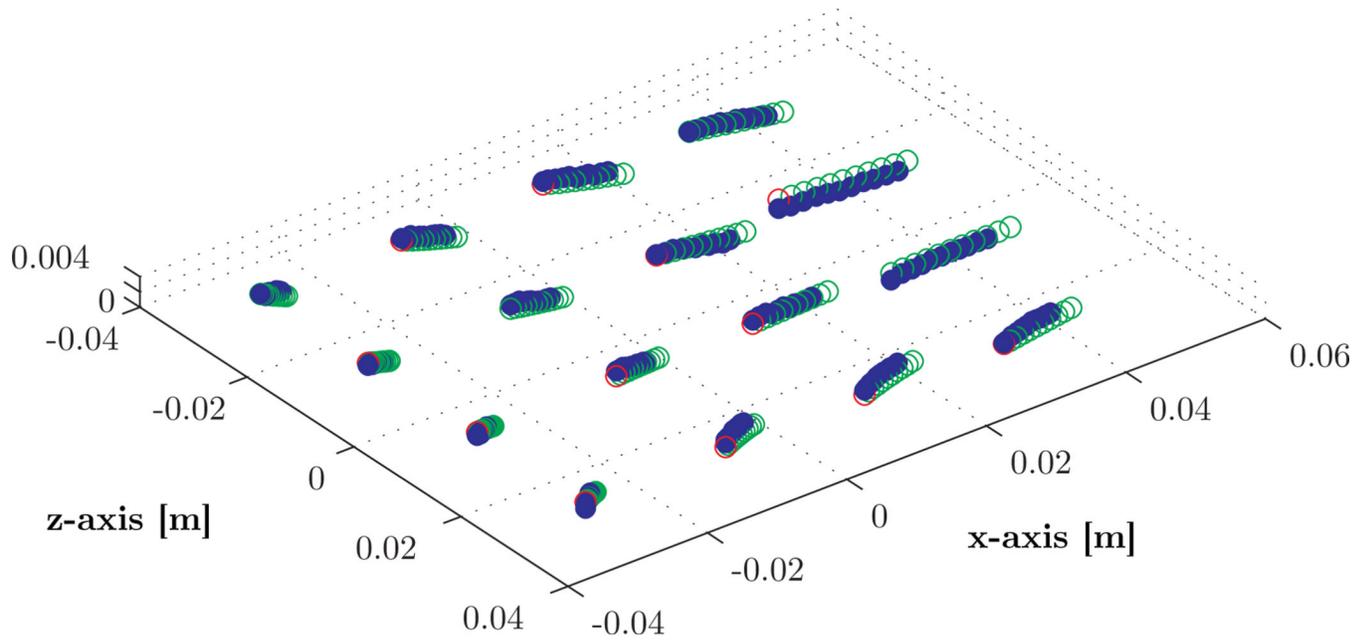
Fig. 7.
The trajectories of fiducial markers from the experiment with Ecoflex 0030 1:1:0 ratio. The solid circles are the trajectories of the points of interest from the stereo cameras, the hollow circles are the trajectories obtained from the simulation using the estimated parameters.
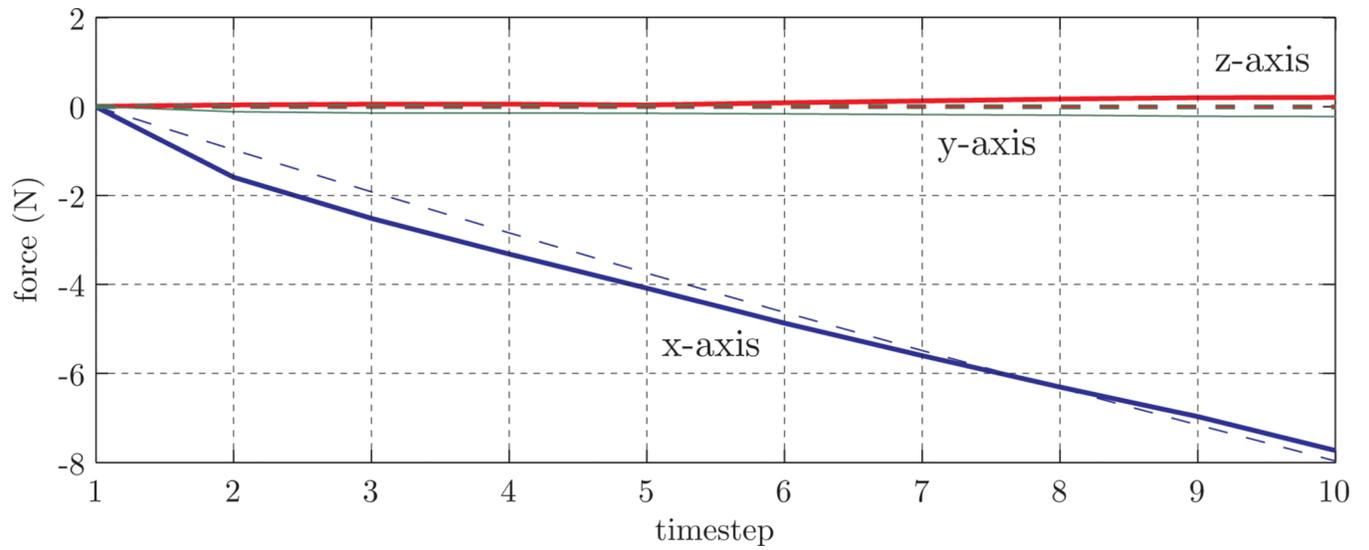
Fig. 8.
The interaction force profile of the experiment with Ecoflex 0030 1:1:0 ratio. The solid lines represent the actual force data from force sensor in x-y-z and the dash lines represent the force profiles obtained from the simulation using the estimated parameters.

TABLE I

Estimation results when accurate tissue and manipulation geometry measurements are available. The computation time is represented as total time, which is the sum of the time for prescaling (9), and time for the actual minimization (8). RMSE stands for root mean square error.

Case	Case 1	Case 2
Young's Modulus (kPa)	15.18	14.98
Poisson's Ratio	0.4897	0.4849
Iterations (Function Counts)	9(30)	15(46)
Time (s) (prescaling+min)	2452(1469+983)	773 (450+90)
RMSE of		
the fiducial's position (m)	4.32e–6	8.30e–5
the force profile (N)	6.73e–5	2.37e–3

TABLE II

Evaluations of the method at different fractal scale levels.

Fractal Max Height Scale	2%	4%	8%
Young's Modulus (kPa)	17.00	19.40	23.97
Poisson's Ratio	0.4693	0.4654	0.4607
Iter. (Func. Counts)	11(34)	14(42)	4(12)
Time (s) (prescaling+min)	375 (227+148)	897(729+168)	956(785+171)
RMSE of			
the fiducial's position (m)	1.15e–4	1.25e–4	1.36e–4
the force profile (N)	1.69e–3	1.85e–3	2.17e–3

TABLE III

Evaluations of the scheme at assuming incorrect grasping points. The parameters and other values are the results from 20 random experiments

Standard Deviation	5 mm	10 mm	20 mm
Young's Modulus (kPa)	13.82 ± 12%	12.06 ± 27%	13.33 ± 62%
Poisson's Ratio	0.4677 ± 4%	0.4574 ± 9%	0.3960 ± 28%
Time (s)	966 ± 27%	1445 ± 79%	1023 ± 60%
RMSE of			
the fiducial's position (m)	6.22e–4 ± 65%	1.71e–3 ± 79%	2.94e–3 ± 76%
the force profile (N)	4.22e–2 ± 63%	1.48e–1 ± 63%	1.63e–1 ± 107%

TABLE IV

The results when the gripper position control signal was corrupted with different noise levels. The parameters and other values are the results from 20 random experiments

Standard Deviation	10%	25%	50%
Young's Modulus (kPa)	14.65 ± 2%	13.88 ± 8%	13.41 ± 19%
Poisson's Ratio	0.4852 ± 2%	0.4733 ± 6%	0.4508 ± 13%
Time (s)	1174 ± 23%	1510 ± 36%	1190 ± 45%
RMSE of			
the fiducial's position (m)	4.14e–4 ± 30%	1.01e–3 ± 29%	2.42e–3 ± 37%
the force profile (N)	3.05e–2 ± 44%	7.66e–2 ± 34%	1.83e–1 ± 66%

TABLE V

Parameter Estimation under Complex Motions

Motion Types	"Tangent Pull" "	In-Plane Tangent Pull"
Young's Modulus (kPa)	14.84	14.95
Poisson's Ratio	0.4845	0.4847
Time (s)	1715(1098+618)	3114(2750+364)
Iter. (Func. Counts)	18(54)	9(27)
RMSE of		
the fiducial's position (m)	1.00e–4	8.60e–5
the force profile (N)	1.77e–3	3.00e–3
Motion Types	"Gradual Tangent Pull"	"Side Pull"
Young's Modulus (kPa)	15.09	15.85
Poisson's Ratio	0.4720	0.4495
Time (s)	3057(2215+843)	885(869+16)
Iter. (Func. Counts)	8(29)	1(3)
RMSE of		
the fiducial's position (m)	2.17e–4	1.36e–4
the force profile (N)	2.06e–2	1.64e–2
Motion Types	"Twist and Pull"	
Young's Modulus (kPa)	15.06	
Poisson's Ratio	0.4762	
Time (s)	1604(1014+590)	
Iter. (Func. Counts)	17(51)	
RMSE of		
the fiducial's position (m)	1.68e–4	
the force profile (N)	9.99e–3	

TABLE VI

The parameter values estimated in the experiments by the proposed method for different tissue phantom materials. (A:B:T is proportion of part A of the silicone, part B of the silicone and silicone thinner by mass.)

Material Types (A:B:T)	Ecoflex 1:1:0	Ecoflex 1:1:2
Young's Modulus (kPa)	27.04	6.493
Poisson's Ratio	0.4287	0.42359
Time (s) (prescaling+min)	856(715+141)	801(676+125)
Iter. (Func. Counts)	12(36)	12(37)
RMSE of		
the fiducial's position (m)	1.59e–3	2.09e–3
the force profile (N)	1.31e–1	2.42e–2